

The Local Effect Model – Principles and Applications

Thomas Friedrich¹, Marco Durante^{1,2}, Michael Scholz¹

¹ GSI Helmholtzzentrum für Schwerionenforschung, Planckstraße 1, 64291 Darmstadt, Germany

² Technische Universität Darmstadt, Hochschulstraße 6, 64289 Darmstadt, Germany

1. Abstract

One major rationale for the application of heavy ion beams in tumor therapy is their increased relative biological effectiveness (RBE) in the Bragg peak region. For dose prescription, the increased effectiveness has to be taken into account in treatment planning. Hence, the complex dependencies of RBE on the dose level, biological endpoint, position in the field etc. require biophysical models, which have to fulfill two important criteria: simplicity and precision. High precision is required since steep gradients in the dose response curves are observed for most tumor and normal tissues; thus, even small uncertainties in the estimation of the biologically effective dose can transform into large uncertainties in the clinical outcome.

In this contribution we will describe the so called 'Local Effect Model' (LEM), that has been successfully applied within treatment planning in the GSI pilot project for carbon ion tumor therapy and is now also implemented in a commercially available treatment planning system. The model is based on the knowledge of charged particle track structure in combination with the response of the cells or tissues under consideration to conventional photon radiation. Due to the high precision, the LEM seems to be adequate for the calculation of stochastic radiation effects, i.e. in the framework of radiation protection in addition to applications in tumor therapy.

2. Introduction

The relative biological effectiveness (RBE) of charged particle beams depends on several factors like particle type and energy, dose level, position in the treatment field and the cell or tissue type under consideration (Blakely et al. 1979, Weyrather et al. 1999, Furusawa et al. 2000). These systematic dependencies of the RBE have to be considered in treatment planning when using charged particle beams for therapy. As a consequence, RBE values are expected to be patient specific and cannot adequately be represented by a single number for conversion of absorbed dose to biologically effective or photon equivalent dose, which is defined here by the product of absorbed dose and RBE. For treatment planning, RBE values have thus to be estimated as precisely as possible.

In principle, two approaches can be followed: an experimental approach and a modeling approach. For the experimental approach, the systematic dependencies of RBE have to be measured with high accuracy for a large number of different irradiation conditions. Therefore, interpolation or extrapolation of the data is required to represent all clinically relevant conditions with respect to beam energies, size of the target volume, dose levels etc. Moreover, because the systematic dependencies can only be measured with sufficiently high resolution in terms of beam energy and LET in in-vitro systems, procedures have to be defined how to derive clinical RBE values for more complex tissue systems from the measured in-vitro data.

The second approach is based on biophysical modeling. The goal here is to develop a model which should be able to predict the response to charged particle radiation for all clinically relevant situations. These include clonogenic survival as the major determinant of tumor control as well as more complex endpoints like normal tissue complications. The model could be based either on first principles or on a restricted set of input data, for which the model could serve as a tool for the extrapolation to a more general case. If for instance the photon dose response curve is used as input for the model, it would ultimately allow linking the treatment planning for charged particle beams to the clinical experience with photon radiation.

The five facilities worldwide currently treating cancer patients with carbon ion beams are using different strategies. At the Japanese facilities in Chiba (HIMAC) and Hyogo (HIBMC), a more experimentally oriented approach is used (Kanai et al. 1997, Kagawa et al. 2002), similar to that used for the earlier clinical trials at the BEVALAC (Petti et al. 1991a, Petti et al. 1991b). This approach also includes a link to the clinical experience with neutrons, which show similar radiobiological characteristics as carbon beams at the end of their penetration depth. Recently though, also biophysical modeling based on the microdosimetric-kinetic model (MKM) (Hawkins1996, Hawkins1998) has been introduced into the treatment planning procedure at HIMAC, specifically for applications of scanned beams (Inaniwa et al. 2010). At GSI/Darmstadt, the Local Effect Model (LEM) has been developed and implemented for treatment planning within the pilot project performed at GSI. This model has also been implemented in commercially available treatment planning systems, that are used at HIT (Heidelberg) and CNAO (Pavia) and are described in more detail in the following (Scholz et al. 1997, Elsässer et al. 2007, Elsässer et al. 2008, Elsässer et al. 2010, Friedrich et al. 2012). It must be emphasized here, that any model implemented in a clinical setting has to be extensively tested by comparison with representative experimental data *in-vitro* and *in-vivo*. If a model is verified by sufficient agreement between model predictions and experimental data, it allows extrapolation to any specific treatment condition.

In the following, we will introduce the concept of the LEM, describe the major steps of development over the last years and present typical examples for the application of the LEM.

3. The Local Effect Model (LEM)

Basic Concepts

The ‘Local Effect Model’ (LEM) aims to derive the biological effects of ion radiation from the response of cells or tissues to photon radiation, thus efficiently exploiting the large data base collected with conventional radiation. It makes use of the concept of the “local dose”, which is defined as the expectation value of the energy deposition at any position in the radiation field for a given pattern of particle trajectories. The main assumption of the LEM is that equal local doses should lead to equal local effects, independent on the radiation quality. This local dose is derived from an amorphous track structure representation of the energy deposition as a function of the radial distance to the particle trajectory. The effectiveness of particles is thus calculated based on the microscopic local dose distribution pattern of ion traversals within the cell nucleus, assuming the nucleus to be the sensitive target for the observed radiation effects. (Figure 1)

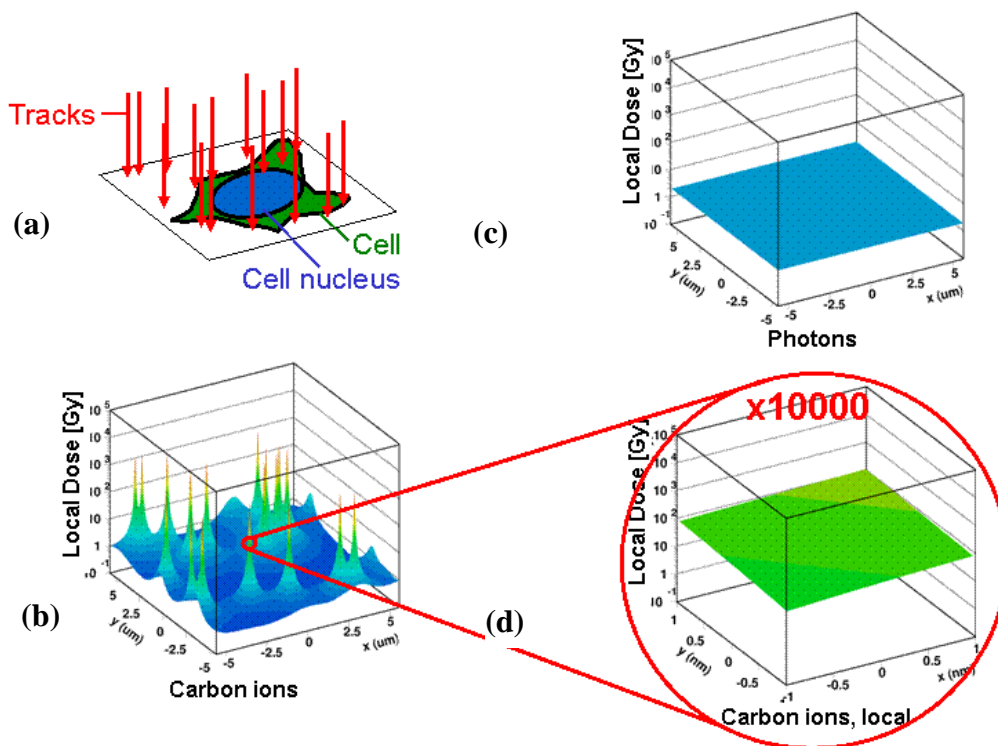


Figure 1:

Comparison of the microscopic local dose distributions of carbon ions and photons for the same macroscopic dose of 2 Gy. For a random distribution of particle traversals through a cell as depicted in (a) the corresponding local dose distribution is characterized by extremely high spikes close to the particle trajectory (b). In contrast, for photons the distributions is expected to be flat (c). Locally, i.e. in nm dimensions, the distributions of particles can also be approximated by a flat distribution (d), thus allowing the link to the photon distribution.

Development and improvements: LEM I – LEM III

For a local dose d_{loc} , in the first implementation of the model (LEM I) (Scholz et al. 1997) the local biological effect is derived directly from the corresponding photon dose response curve denoted as $S_\gamma(D)$, where S represents the survival at dose D . This response curve is represented by the linear-quadratic (LQ) parameters α_γ and β_γ for the specific biological endpoint under consideration, which are known from experiments or clinical data. Since the linear-quadratic description is only valid for doses in the order of 5 – 10 Gy (Astrahan 2008), a correction for $S(D)$ was introduced in order to account for a transition to a linear shape at higher doses $D > D_t$, where D_t denotes the ‘threshold’ dose for the transition.

For the prediction of cell killing, the biological effectiveness of any ion radiation field can then be derived from the quantity

$$\overline{N_{l,ion}} = \int \frac{-\ln S_x(d(x,y,z))}{V_{Nucleus}} dV_{Nucleus} \quad (1)$$

where $S_X(D)$ represents the effect after photon radiation as a function of dose D , $d(x,y,z)$ is the distribution of the local dose within the critical target, assumed to be the cell nucleus and V_{Nucleus} is the volume of the cell nucleus.

The term $-\ln S_X(D)$ can be interpreted as the mean number of lethal events produced per cell by photons at a dose D ; the integrand in eq. (2-13) thus represents a local density of lethal events at a given position (x,y,z) in the nucleus. Integration of this event density over the volume of the nucleus for a given local dose distribution pattern deposited by particle traversals results in the mean number of lethal events $N_{l,lon}$ per cell induced by these traversals.

Assuming a Poissonian distribution of the number of lethal events around this mean value, the surviving fraction is determined by the fraction of cells with no lethal events and thus by

$$S_{lon} = e^{-\overline{N_{l,lon}}} \quad (2)$$

By comparison of the photon dose D_γ leading to the same survival, i.e. $S_\gamma = S_{lon}$ RBE values can then be derived from

$$RBE = \frac{D_\gamma}{D_{lon}} \Big|_{Isoeffect} \quad (3)$$

The full integration as indicated in (2-13) would be too time consuming for purposes of therapy planning; therefore, approximations have been introduced, which are described in more detail in (Scholz et al. 1997, Krämer et al. 2000b, Scholz et al. 2006).

Although the predictions of the LEM I were in reasonable agreement with experimental and clinical data e.g. for carbon ion irradiation in a spread-out Bragg peak (SOBP), where deviations were in the order of 10-20% for therapy relevant conditions, larger systematic deviations were observed for high-energy, low-LET ions and lighter ions as e.g. protons or helium ions when using the model parameters optimized for the description of carbon ions. Consequently, improvements have been implemented, which were aiming at reducing these systematic differences. In the LEM II (Elsässer et al. 2007), the increased yield of DSB, resulting from the induction of DNA single strand breaks in close vicinity (<25 bp) is taken into account, leading to a further enhancement of the biological effects at very high local doses (>1000 Gy). Furthermore, since a considerable fraction of the biological damage is induced by the indirect effect, the effects of radical diffusion have been considered in more detail in the LEM II, that lead to a “wash out” of the extremely spiked local dose distribution in the particle track center.

A further refinement was achieved with the implementation of a more detailed track structure description, now including an energy dependent extension of the track core (LEM III, (Elsässer et al. 2008)). This energy dependence further increased the gradient of RBE along the penetration depth and with that led to a better agreement of the model predictions with experimental data.

Generalization: LEM IV

A key feature of the earlier versions LEM I – LEM III as described above is the direct link of the local dose deposition pattern to the photon dose response curve describing the observable

endpoint under consideration. For the extension recently reported (LEM IV, (Elsässer et al. 2010)), we have introduced an intermediate step, based on the premise that the *final biological response* of a cell to radiation is directly linked to the *initial spatial DNA damage distribution* induced by radiation rather than the local dose distribution itself. We assume that the microscopic spatial distribution of DNA damage, namely double strand breaks (DSB) and in particular their local density, represents the relevant measure determining the fate of a cell after radiation insult. Furthermore, in line with the general concepts of the LEM, we assume that similar DSB patterns should lead to similar effects, independent of the radiation quality leading to these patterns.

Although of course a strong correlation between the energy deposition pattern and the spatial damage distribution pattern is expected and thus the distinction made above seems to be quite subtle, actually under certain conditions both views lead to significantly different conclusions. This can be illustrated by means of the examples shown in Fig. 2.

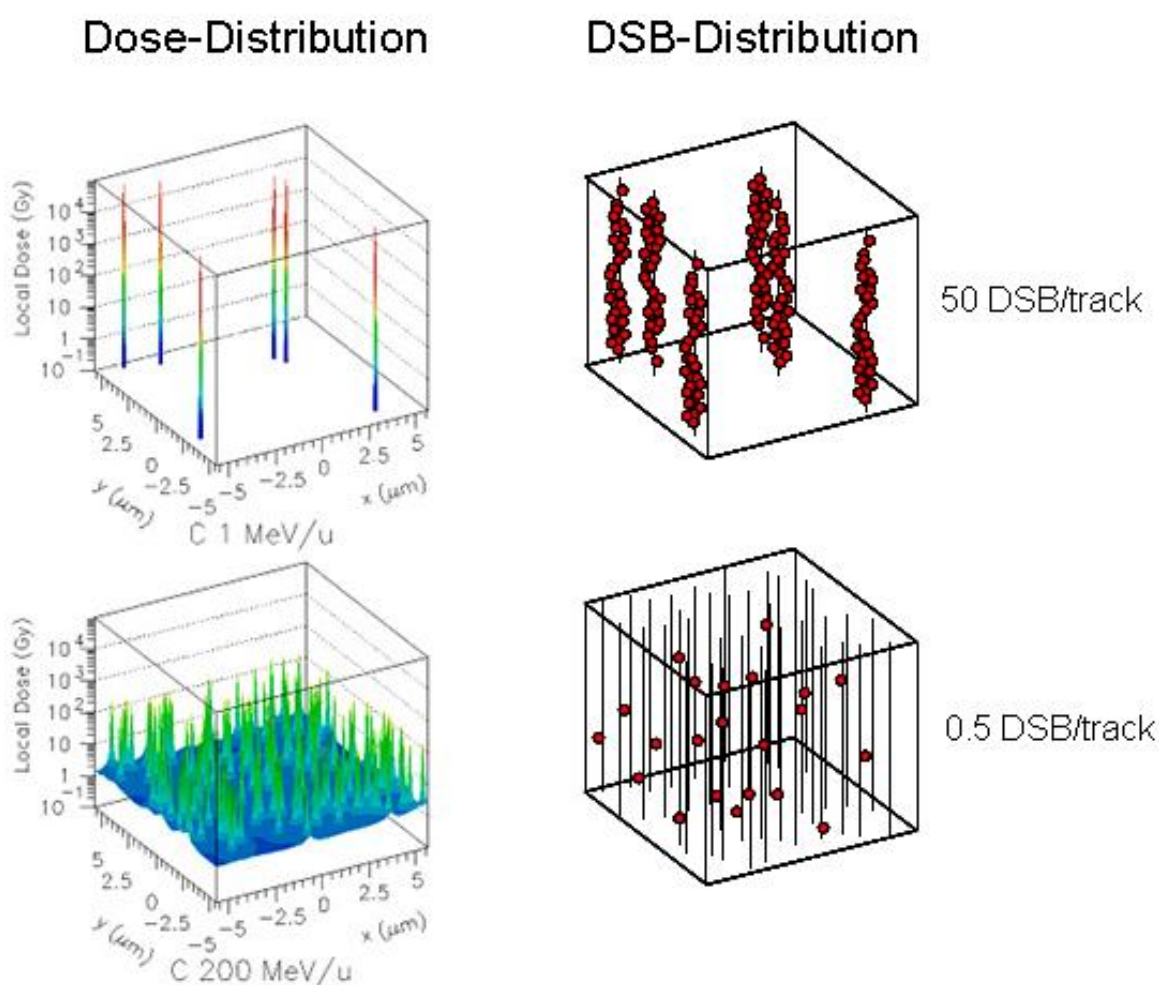


Figure 2:

Schematic comparison of the local dose distributions (left) and corresponding spatial DSB distributions (right) for low energetic (top) and high energetic (bottom) carbon ions. Assumed DSB yields are 50 DSB and 0.5 DSB for the low energetic and high energetic ions, respectively.

The figure schematically compares the microscopic dose distribution (left side) for low energetic and high energetic carbon ions of comparable macroscopic dose levels, respectively, with the corresponding distribution of double strand breaks. For low energetic ions, having very high LET, the local dose distribution is extremely peaked, and as a result of the extremely high local dose deposition and the narrow track diameter the high number of DSB are concentrated along the particle trajectory. Here, both the high local dose distribution as well as the clustered DSB distribution intuitively indicate an enhanced effectiveness of the carbon ions.

This picture changes when analyzing distributions for the high energetic ions. Here, the local dose still shows significant peaks at the center of the individual tracks, although the space between individual tracks is now filled with a “bath” of low local doses which originate from the overlap of the outer regions of the individual tracks, which have a comparably large diameter at these high energies. However, assuming that for example at these low LET values an individual particle produces only 0.5 DSB on average, the resulting pattern of DSB obeys a random distribution according to the random pattern of particle traversals. Now, different conclusions can be drawn from the local dose deposition pattern and the DSB pattern. The spikes in the local dose distribution would still suggest an increased effectiveness of the particles. However, since the DSB pattern is random, it cannot be distinguished from the pattern that would be induced by photon radiation, and thus the same effectiveness is expected on the basis of the DSB distribution.

Since the cell actually responds to the damage induced by the particle traversals, but not directly to the energy deposition, the spatial DSB distribution pattern is considered to be the more relevant measure to assess the effectiveness of different radiation qualities. The induction of clustered damages is an important aspect that is reflected in the spatial DSB distribution pattern.

In order to assess the similarity of DSB distributions, specific measures have to be defined. In the LEM IV, these are related to the structure of chromatin organization in the cell nucleus. It is assumed that so called ‘giant loops’ of DNA (Yokota et al. 1995, Solovjeva et al. 1998), comprising about 2 Megabase pairs (Mbp) DNA length, represent the critical structure of the DNA (Ostashevsky 1998, Johnston et al. 1998). We then distinguish two types of damage, namely that either only a single DSB (‘isolated DSB’, iDSB) is induced in such a loop structure or two or more DSB (‘clustered DSB’, cDSB) are induced. It is hypothesized that cDSB lead to a significant higher probability of e.g. cell killing as compared to iDSB, since for iDSB the DNA on both sides of the DSB is still attached to the nuclear matrix, and thus repair is expected to be facilitated in general in this case. In contrast, for cDSB one or more DNA fragments can be removed from the loop, which are not any longer attached to the nuclear matrix and thus correspondingly difficult to repair (Fig. 3).

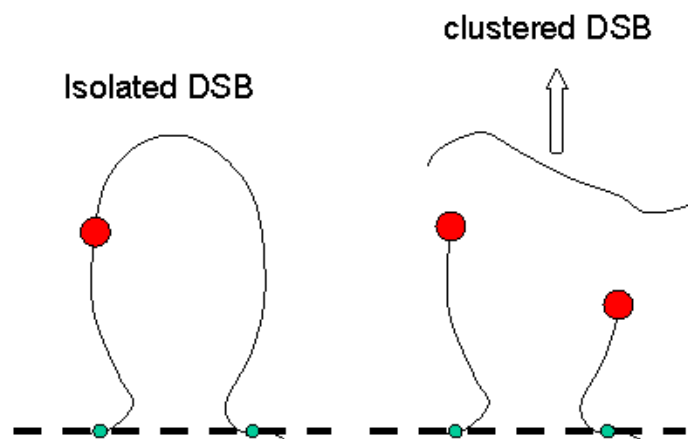


Figure 3

Schematic representation of the chromatin giant loop structure (adapted from Yokota et al.) and the consequence of isolated or clustered DSB within loops. For simplicity, only the essential topology of chromatin loop structure is shown; the actual conformation of individual loops includes additional complicated 3-dimensional folding.

Assuming that damage induced in different DNA loops can be considered to act independently, the total number of loops with iDSB and cDSB, respectively, represents a measure of the clustering of the DSB induced by a given dose deposition, as defined by the cluster-index C :

$$C = \frac{N_{cDSB}}{N_{iDSB} + N_{cDSB}} \quad (4)$$

where N_{cDSB} and N_{iDSB} represent the number of loops with isolated and clustered DSB, respectively.

The calculation of the spatial DSB distribution is based on the local dose derived from the radial dose profile described above and used already for the previous versions of the LEM. Assuming a homogenous distribution of the DNA within the nucleus as a first approximation, the mean number of DSB in any small subvolume of the nucleus can be derived from experimental photon data, which indicate that the yield of radiation-induced DSB is approximately 30 DSB/Gy/cell. Based on the local average number of DSB, spatial DSB distributions are then determined by means of Monte-Carlo techniques, i.e. actual DSB distributions are determined by considering the amorphous track structure pattern as the probability density distribution of DSB.

Assuming a homogenous distribution of DNA within the nucleus, the amount of DNA contained in a loop (approx. 2 Mbp) can be attributed to a subvolume of the nucleus, based on the knowledge of the total DNA content (approx. 6×10^9 Mbp in mammalian cells) and the typical volume of the nucleus (approx. $500 \mu\text{m}^3$). In order to determine the number of isolated

and clustered DSB, the cell nucleus is divided into cubic shaped subvolumes with 540 nm side length, corresponding to the volume covered by a 2 Mbp DNA content when assuming a homogenous distribution of DNA within the nucleus. The number of DSB in each subvolume is determined according to the local dose distribution within the subvolume and the subvolumes are then classified as isolated DSB or clustered DSB if exactly one DSB or two or more DSB are induced in a subvolume, respectively.

In order to determine the biological effect of a given spatial DSB pattern, in a first step the photon dose that leads to the same damage complexity C , i.e. the same relative composition of iDSB and cDSB, is determined. In a second step, the effect produced by that photon dose is appropriately scaled according to the total number of iDSB or cDSB that are induced by a particle traversal and the photon dose, respectively. As a result, the number of lethal events induced by a single particle traversal is obtained.

This procedure permits calculation of the effect of a single particle traversal, defining the effectiveness at low doses and thus the α_1 term of the linear-quadratic representation of the dose response curve. The β_1 -term can then be estimated according to the approximation described in (Krämer et al. 2006). This approximation has been introduced since full simulations of dose response curves would be unfeasible for applications in the framework of treatment planning; this was mainly due to the extremely time consuming calculations.

The concept of the LEM IV also allows implementation of a detailed, full simulation for arbitrary random particle traversal patterns (Friedrich et al. 2012). Compared with the single-particle approximations, typically higher β -values are predicted in the intermediate LET region, and work is in progress to analyse in more detail the impact of these differences on the level of track-segment conditions as well as for clinical applications using spread-out Bragg peaks.

4. Applications

For treatment planning, the accurate prediction of RBE for tumor cell killing and normal tissue effects is essential. The model has thus been validated based on large sets of experimental data (Elsässer et al. 2008, Elsässer et al. 2010, Friedrich et al. 2012b). Figure 4 shows a comparison of model predictions with experimental data obtained with helium and carbon ions for the different model versions. Interestingly, the model improvements had little effect on the shape of the RBE-LET-relationship at high LET values beyond the maximum of RBE. The main impact is observed in the rising part of the RBE-LET-curve, where essentially the gradient is affected, which consequently also affects the rise of RBE with penetration depth in a typical spread out Bragg peak (SOBP). In general, for the most recent implementation (LEM IV) a very good agreement is observed between the predictions and the experimental data.

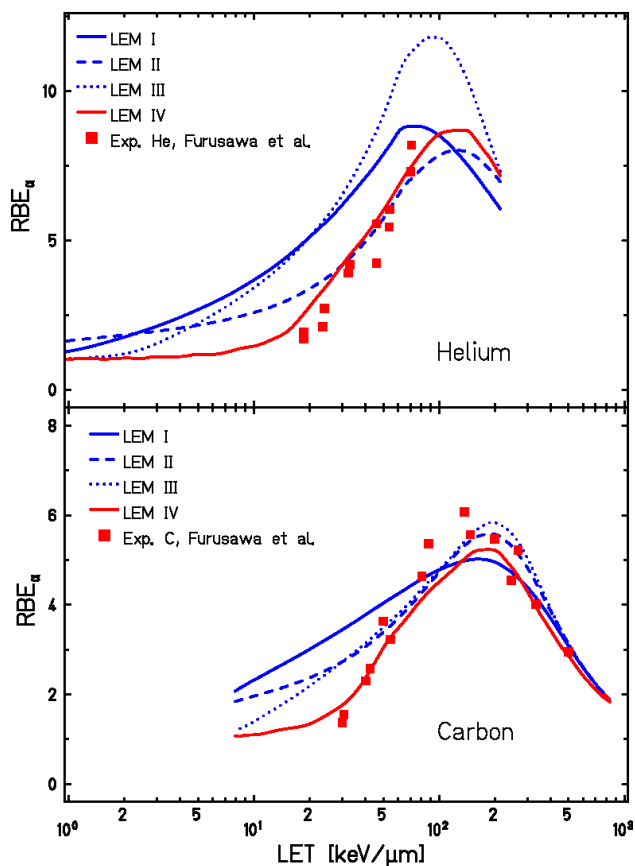


Figure 4:

Comparison of RBE predictions for different LEM versions with experimental data for He irradiation (top) and C irradiation (bottom). Experimental data were taken from Furusawa et al. (2000).

With respect to normal tissue toxicity, application of the LEM needs some generalization because typically normal tissue responses cannot be easily traced back to effects of cell killing, in particular for tissues like CNS where cell proliferation normally does not occur and thus cell survival is not defined in the sense of the clonogenic assay.

However, dose response curves for normal tissue effects also typically can be described in terms of the linear-quadratic model, and thus hypothetical “survival” curves can be constructed from the known α , β or α/β -values, and then the corresponding RBE values can be calculated in analogy to the procedure applied for cell killing.

Since the CNS represents a critical tissue which frequently limits the dose given to the tumor, such as in the case of head and neck tumors, as they were mainly treated within the pilot project, tolerance of the spinal cord has been studied in pre-clinical in-vivo experiments (Debus et al. 2003, Karger et al. 2006). Figure 5 presents a comparison of the RBE values predicted by the LEM IV, assuming an α/β -value for photon radiation of 2 Gy, with the experimental data as reported by Karger et al. (2006). Also here, a significant improvement is achieved with the most recent implementation of the LEM (Grün et al. 2012).

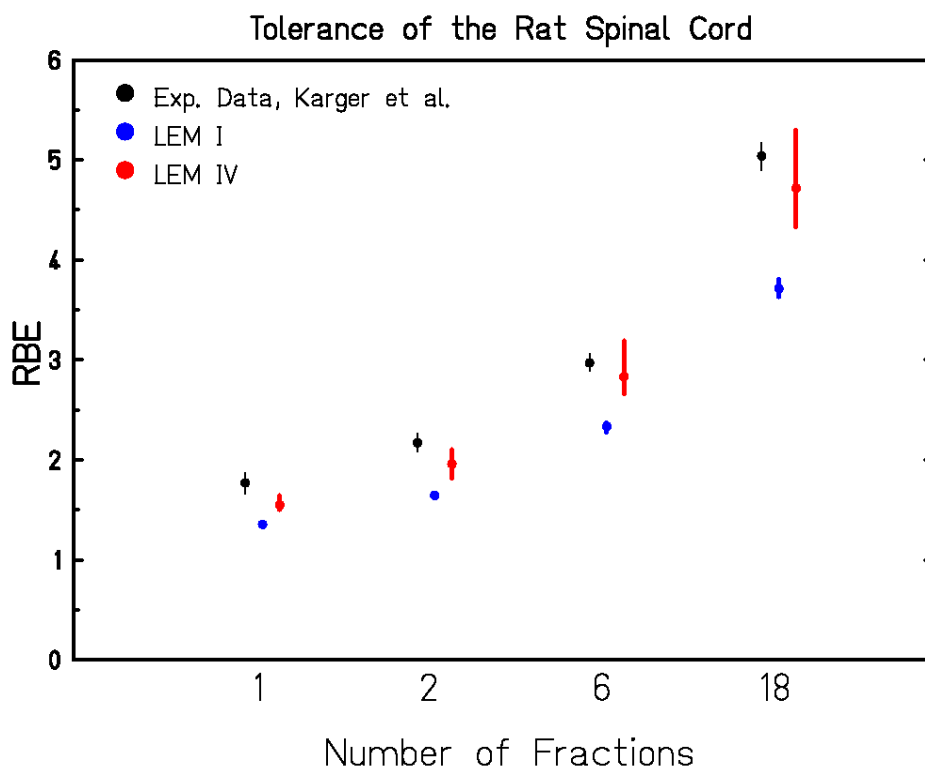


Figure 5:

Predictions of LEM I and LEM IV for the RBE for the tolerance of the rat spinal cord in comparison to experimental data reported by Karger et al. Redrawn after Grün et al., PMB 2012. Vertical bars for experimental RBE values represent error bars; vertical bars for LEM calculations represent uncertainties due to positioning uncertainties of +/- 1mm of the spinal cord and the RBE gradient within the spread-out Bragg peak.

5. Potential applications in radiation protection and space research

Although primarily developed in the framework of ion beam therapy, conceptually the LEM is not restricted to this type of application. Applications in the field of radiation protection seem feasible, although there may be reasons for adaptations.

The closest link to aspects of radiation protection exists in the case of an acute radiation insult, because the doses are comparably high and the mechanisms of radiation damage are similar to those leading to early and late normal tissue response in radiation therapy. Under these conditions, the model should be applicable in principle without major modifications.

In contrast, applications to effects of low doses and extremely protracted irradiation as they will likely occur on long space flights and their corresponding relevant endpoints require extensions of the model mainly in two aspects:

- An important endpoint of interest for radiation protection is cancer induction. Here in particular the competition and balance between cell killing and cell transformation has to be considered. The corresponding photon dose response curve for both endpoints can be described in terms of the linear-quadratic model. Therefore, the LEM can be used to separately calculate dose response curves for killing and transformation

induction, and the probability of inducing viable transformed cells can be derived from the appropriate combination of both effects. First attempts in this direction have been made with earlier versions of the model (Scholz and Elsässer 2007a) and have also been tested with the most recent model version by comparison with the large data sets reported for low energy charged particle radiation (Miller et al. 1995) and high energy particle radiation (Yang et al. 1985). Preliminary results show reasonable agreement between prediction and experimental data, particularly with the latest model version.

- Dose rate effects have to be included. Here, the more mechanistic concept of the LEM IV as compared to the previous model versions makes extension to dose rate effects particularly suitable. Since the LEM IV is explicitly based on consideration of the induction of DSB and their spatial distribution, repair and rejoining of DSBs can also be included here based on kinetic parameters derived from experimental data. This allows consideration of the time sequence of induction and repair of DSB in more detail and thus ultimately prediction of dose rate effects. Currently projects are ongoing to implement dose rate effects in the LEM. In the meantime we have shown that the basic concept of the LEM, namely the description of the effect in terms of iDSB and cDSB, also allows for the description of photon dose response curves (Friedrich et al. 2012). We first implemented the concept to describe dose rate effects for photon irradiation and could demonstrate its applicability [L. Herr, submitted to Rad. Res. 2013]. Based on the same strategy for rejoining and repair of iDSB and cDSB, respectively, the transfer to ion beam radiation is conceptually straightforward. The first results of this implementation are expected to be available soon.

6. Summary and Conclusion

The LEM was originally developed in the framework of ion beam therapy. Systematic validation of the model has been performed on the basis of cell survival data (Elsässer et al. 2007, Elsässer et al. 2008, Elsässer et al. 2010) and *in vivo* experimental data (Elsässer et al. 2008, Grün et al. 2012). It has been implemented in the treatment planning software TRiP (Krämer et al. 2000a, Krämer et al. 2000b, Krämer et al. 2006), and the predicted RBE values have been shown to be consistent with clinical data for carbon ion beam therapy obtained in the pilot project performed at GSI (Scholz et al. 2006, Schulz-Ertner et al. 2007, Schlamp et al. 2011). I

In particular the consistency with the clinical data demonstrates that despite its simplicity the model is able to accurately predict the biological response of complex tissue systems to high-LET radiation. The key to the model's success lies in the link to the photon dose response curve, which already contains all relevant information - including the underlying complex biological processes - as a type of a "black box".

Extensions of the model with respect to the specific endpoints and boundary conditions relevant for radiation protection issues seem feasible, and currently projects are ongoing that are aimed at demonstrating the applicability of the model in this framework.

7. References

- Astrahan M. Some implications of linear-quadratic-linear radiation dose-response with regard to hypofractionation. *Med Phys* 2008; 35:4161-4172
- Blakely EA, Tobias CA, Yang TC, Smith KC, and Lyman JT. Inactivation of human kidney cells by high-energy monoenergetic heavy-ion beams. *Radiat Res* 1979; 80:122-160
- Debus J, Scholz M, Haberer T, Peschke P, Jakel O, Karger CP et al. Radiation tolerance of the rat spinal cord after single and split doses of photons and carbon ions. *Radiat Res* 2003; 160:536-542
- Elsässer T, Krämer M, and Scholz M. Accuracy of the local effect model for the prediction of biologic effects of carbon ion beams in vitro and in vivo. *Int J Radiat Oncol Biol Phys* 2008; 71:866-872
- Elsässer T and Scholz M. Cluster effects within the local effect model. *Radiat Res* 2007; 167:319-329
- Elsässer T and Scholz M. Biophysical models in ion beam therapy. *Adv Space Res* 2007a; 40:1381-1391
- Elsässer T, Weyrather WK, Friedrich T, Durante M, Iancu G, Krämer M et al. Quantification of the relative biological effectiveness for ion beam radiotherapy: direct experimental comparison of proton and carbon ion beams and a novel approach for treatment planning. *Int J Radiat Oncol Biol Phys* 2010; 78:1177-1183
- Friedrich T, Scholz U, Elsässer T, Durante M, and Scholz M. Calculation of the biological effects of ion beams based on the microscopic spatial damage distribution pattern. *Int J Radiat Biol* 2012; 88:103-107
- Friedrich T, Scholz U, Elsässer Th, Durante M, Scholz M. Systematic analysis of RBE and related quantities using a database of cell survival experiments with ion beam irradiation. *J Radiat Res* 2012b
- Furusawa Y, Fukutsu K, Aoki M, Itsukaichi H, Eguchi-Kasai K, Ohara H et al. Inactivation of aerobic and hypoxic cells from three different cell lines by accelerated (3)He-, (12)C- and (20)Ne-ion beams. *Radiat Res* 2000; 154:485-496
- Grün R, Friedrich T, Elsässer T, Krämer M, Zink K, Karger CP et al. Impact of enhancements in the local effect model (LEM) on the predicted RBE-weighted target dose distribution in carbon ion therapy. *Phys Med Biol* 2012; 57:7261-7274
- Hawkins RB. A microdosimetric-kinetic model of cell death from exposure to ionizing radiation of any LET, with experimental and clinical applications. *Int J Radiat Biol* 1996; 69:739-755
- Hawkins RB. A microdosimetric-kinetic theory of the dependence of the RBE for cell death on LET. *Med Phys* 1998; 25:1157-1170

- Inaniwa T, Furukawa T, Kase Y, Matsufuji N, Toshito T, Matsumoto Y et al. Treatment planning for a scanned carbon beam with a modified microdosimetric kinetic model. *Phys Med Biol* 2010; 55:6721-6737
- Johnston PJ, MacPhail SH, Banath JP, and Olive PL. Higher-order chromatin structure-dependent repair of DNA double-strand breaks: factors affecting elution of DNA from nucleoids. *Radiat Res* 1998; 149:533-542
- Kagawa K, Murakami M, Hishikawa Y, Abe M, Akagi T, Yanou T et al. Preclinical biological assessment of proton and carbon ion beams at Hyogo Ion Beam Medical Center. *Int J Radiat Oncol Biol Phys* 2002; 54:928-938
- Kanai T, Furusawa Y, Fukutsu K, Itsukaichi H, Eguchi-Kasai K, and Ohara H. Irradiation of mixed beam and design of spread-out Bragg peak for heavy-ion radiotherapy. *Radiat Res* 1997; 147:78-85
- Karger CP, Peschke P, Sanchez-Brandelik R, Scholz M, and Debus J. Radiation tolerance of the rat spinal cord after 6 and 18 fractions of photons and carbon ions: experimental results and clinical implications. *Int J Radiat Oncol Biol Phys* 2006; 66:1488-1497
- Krämer M, Jakel O, Haberer T, Kraft G, Scharadt D, and Weber U. Treatment planning for heavy-ion radiotherapy: physical beam model and dose optimization. *Phys Med Biol* 2000a; 45:3299-3317
- Krämer M and Scholz M. Treatment planning for heavy-ion radiotherapy: calculation and optimization of biologically effective dose. *Phys Med Biol* 2000b; 45:3319-3330
- Krämer M and Scholz M. Rapid calculation of biological effects in ion radiotherapy. *Phys Med Biol* 2006; 51:1959-1970
- Miller RC, Marino SA, Brenner DJ, Martin SG, Richards M, Randers-Pehrson G et al. The biological effectiveness of radon-progeny alpha particles. II. Oncogenic transformation as a function of linear energy transfer. *Radiat Res* 1995; 142:54-60
- Ostashevsky J. A polymer model for the structural organization of chromatin loops and minibands in interphase chromosomes. *Mol Biol Cell* 1998; 9:3031-3040
- Petti PL, Lyman JT, and Castro JR. Sensitivity of helium beam-modulator design to uncertainties in biological data. *Med Phys* 1991a; 18:506-512
- Petti PL, Lyman JT, Renner TR, Castro JR, Collier JM, Daftari IK et al. Design of beam-modulating devices for charged-particle therapy. *Med Phys* 1991b; 18:513-518
- Schlamp I, Karger CP, Jakel O, Scholz M, Diding B, Nikoghosyan A et al. Temporal lobe reactions after radiotherapy with carbon ions: incidence and estimation of the relative biological effectiveness by the local effect model. *Int J Radiat Oncol Biol Phys* 2011; 80:815-823
- Scholz M, Kellerer AM, Kraft-Weyrather W, and Kraft G. Computation of cell survival in heavy ion beams for therapy. The model and its approximation. *Radiat Environ Biophys* 1997; 36:59-66

- Scholz M, Matsufuji N, and Kanai T. Test of the local effect model using clinical data: tumour control probability for lung tumours after treatment with carbon ion beams. *Radiat Prot Dosimetry* 2006; 122:478-479
- Schulz-Ertner D, Karger CP, Feuerhake A, Nikoghosyan A, Combs SE, Jakel O et al. Effectiveness of carbon ion radiotherapy in the treatment of skull-base chordomas. *Int J Radiat Oncol Biol Phys* 2007; 68:449-457
- Solovjeva L, Svetlova M, Stein G, Chagin V, Rozanov Y, Zannis-Hadjopoulos M et al. Conformation of replicated segments of chromosome fibres in human S-phase nucleus. *Chromosome Res* 1998; 6:595-602
- Weyrather WK, Ritter S, Scholz M, and Kraft G. RBE for carbon track-segment irradiation in cell lines of differing repair capacity. *Int J Radiat Biol* 1999; 75:1357-1364
- Yang TC, Craise LM, Mei MT, and Tobias CA. Neoplastic cell transformation by heavy charged particles. *Radiat Res Suppl* 1985; 8:S177-S187
- Yokota H, van den Engh G, Hearst JE, Sachs RK, and Trask BJ. Evidence for the organization of chromatin in megabase pair-sized loops arranged along a random walk path in the human G0/G1 interphase nucleus. *J Cell Biol* 1995; 130:1239-1249